Earth Planets Space, **58**, 5–21, 2006

Coseismic and postseismic surface displacements of the 10 December 2003 (M_W 6.5) Chengkung, eastern Taiwan, earthquake

Horng-Yue Chen, Shui-Beih Yu, Long-Chen Kuo, and Chi-Ching Liu

Institute of Earth Sciences, Academia Sinica, P.O. Box 1-55 Nankang, Taipei, Taiwan

(Received September 28, 2004; Revised September 2, 2005; Accepted September 2, 2005; Online published January 27, 2006)

The M_W 6.5 Chengkung earthquake occurred in eastern Taiwan at 04:38 UTC on 10 December 2003. The GPS data from eighteen continuously recording stations (CORS) and 86 campaign-surveyed stations (CSS) collected 18 days to 9 months before and 6 days to 4 months after the main shock are utilized to analyze the coseismic and postseismic deformation associated with the Chengkung earthquake. The earthquake resulted from rupturing of the Chihshang fault, a 25-km-long segment of the Longitudinal Valley Fault (LVF). The coseismic horizontal displacements in the hanging wall showed a fan-shape distribution with vectors towards the west. On the other hand, the movements of the revealed a mirror fan-shape with relatively lesser amounts of displacement. The largest coseismic displacement, which reached 126 mm and 263 mm in the horizontal and vertical components, occurred near the epicenter area in the hanging wall. The largest postseismic displacements in 109 days, which approached 59 mm and 68 mm in the horizontal and vertical components, occurred near the surface trace of the Chihshang fault (TAPO) and near the epicenter area (CHEN), respectively. The stations near the Chihshang fault indicated a more significant postseismic displacement than coseismic one.

Key words: Coseismic displacement, postseismic deformation, Chengkung earthquake, Longitudinal Valley Fault.

1. Introduction

A moderate shallow earthquake (M_W 6.5 and named Chengkung earthquake) occurred in eastern Taiwan at 12:38 local time on 10 December 2003 (Fig. 1). According to the Central Weather Bureau (CWB) of Taiwan (CWB earthquake report, 2003), the epicenter was located at 23.07°N, 121.40°E, with a focal depth of 17.7 km. The earthquake caused damage to buildings and bridges in the town of Chengkung and the nearby Tungho district. Analyzing the location of the main shock, the distribution of the aftershocks and their focal mechanisms, it indicated a fault plane with a NNE strike and an east-dipping angle of 30°∼60° extending from surface to a depth of 25 km (Broadband array in Taiwan for seismology (BATS), 2003; Cheng *et al*., 2004). The surface extension of this fault plane is in a good agreement with the surface trace of the Chihshang fault in the southern Longitudinal Valley, a plate suture separating the Central Range of the Eurasian plate to the west and the Coastal Range of the Philippine Sea plate to the east (Teng and Wang, 1981; Page and Suppe, 1981; Angelier *et al*., 1997, 2000).

2. Geodetic Measurements in the Longitudinal Valley Area

In the past two decades, abundant geodetic data have been collected along the Longitudinal Valley area mainly by repeated campaigns using precise trilateration surveys, first-order leveling, and the Global Positioning System (GPS) (Yu and Liu, 1989; Yu *et al*., 1990, 1992, 1997; Yu and Kuo, 2001). The Longitudinal Valley fault, hereafter called LVF, is a high-angle thrust with a left-lateral component and is one of the most active faults in the Taiwan area (Barrier *et al*., 1982; Yu and Liu, 1989; Lee and Angelier, 1993; Angelier *et al*., 1997). Horizontal velocity field derived from the GPS measurements indicated a distinct discontinuity across the LVF with a difference of velocity of about 30 mm/yr (Yu and Kuo, 2001). This horizontal shortening is principally revealed by shallow aseismic slips on the LVF (Yu and Liu, 1989; Yu *et al*., 1990; Lee *et al*., 2003). The creeping behavior of the LVF is prominent, especially in its southern part from Juisui to Taitung (Fig. 2), extending for about 80 km long (Yu and Kuo, 2001). The vertical motion in the western margin of Coastal Range relative to the Longitudinal Valley shows a stable uplift rate of 10∼20 mm/yr (Yu and Liu, 1989). The uplift rate reaches its maximum around Fuli and decreases both southward and northward (Yu and Liu, 1989; Yu *et al*., 1992; Yu and Kuo, 2001).

Beginning 1997, in order to better understand the fault-creep in the southern segment of the LVF, annual GPS surveys as well as first-order precise leveling were conducted. We integrated data from 18 continuously recording GPS stations (CORS) installed by the Institute of Earth Sciences, Academia Sinica (IESAS), the Central Weather Bureau (CWB), and the Ministry of the Interior (MOI), and 41 campaign-surveyed stations deployed by IESAS since 1990. Furthermore, a dense network with 45 monitoring stations in this area has been established since 2001 (Fig. 1). We also carried out repeated precise leveling along two 10

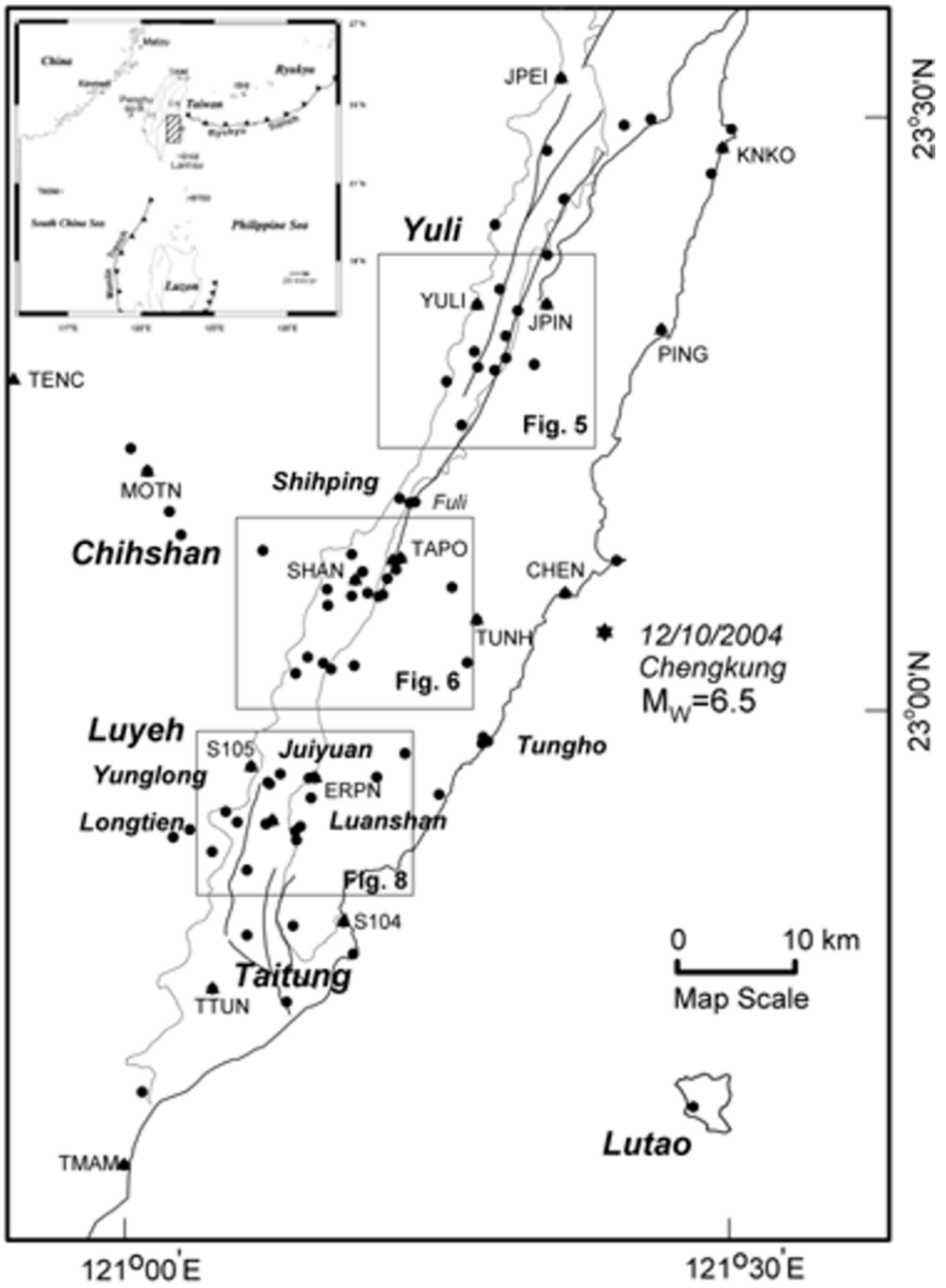

Fig. 1. The 18 continuous GPS stations and 86 campaign-surveyed stations in the study area of southeastern Taiwan.

km-length lines in the Luyeh area (Fig. 1). As a result, the elevation changes of benchmarks can be compared with those obtained from GPS surveys.

Eighteen days after our November 2003 GPS surveys in southeastern Taiwan, the Chengkung earthquake occurred on 10 December 2003 (Day-of-year (DoY) 344). Immediate after the earthquake, the Geodetic Group of the IESAS organized a GPS field survey (DoY 349∼354) around the epicentral area to measure the coseismic and postseismic surface displacements. It is worthy noting that the timing of observation following the main shock played an important role in determining coseismic and postseismic displacements, especially near the fault, where postseismic deformation changed drastically as a function of time (Smith and Wyss, 1968; Williams and Magistrale, 1989; Yu *et al.*, 2003). According to the data recorded by the continuously recording GPS stations before and after the Chengkung earthquake, the coseismic and postseismic displacements of the campaign-surveyed stations can be calibrated by applying the nearby continuous GPS stations (Hwang *et al.*, 2004). Although surface deformation of earthquake or landslide can be determined by the kinematic positioning algorithms (Bock *et al.*, 2000; Remondi and Brown, 2000), however, we choose to adopt the post-processing daily solution algorithm to determine the relative position in the conditions for better reliability and accuracy (Chen *et al.*, 2003).

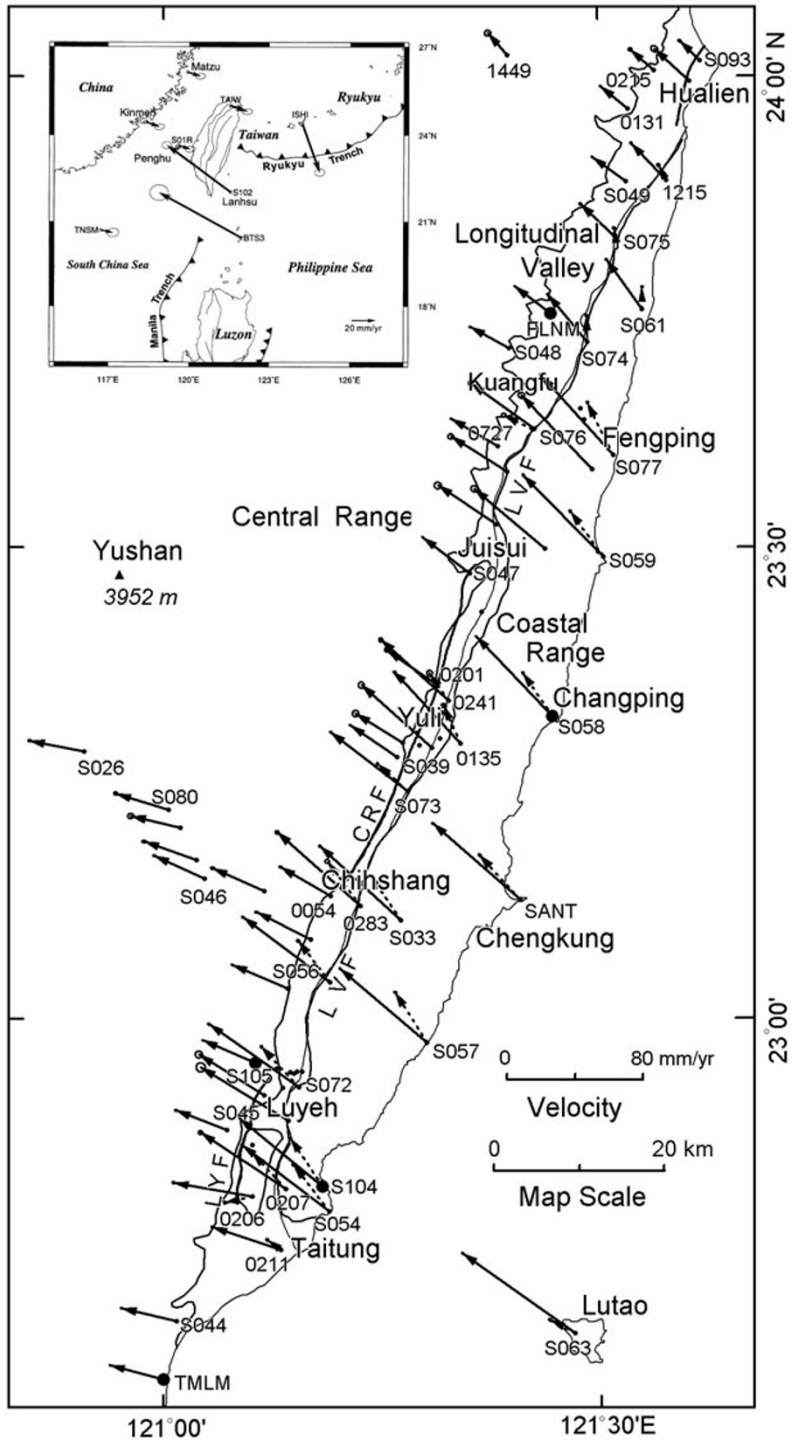

Fig. 2. The velocity field of the inter-seismic period (1992–1999) in eastern Taiwan. The vectors are derived from the GPS measurements with respect to the Paisha station of Penghu Island in the Chinese continental margin. The black dashed arrow in the Coastal Range are velocities with respect to the eastern margin of the Central Range (after Yu and Kuo, 2001).

3. Data Acquisition and Processing

In this study, we used eighteen continuously recording GPS stations (CORS) and more than 86 campaign-surveyed stations (CSS) to detect the crustal motion in the south segment of the LVF (Fig. 1). Thirteen continuous stations (JPEI, KNKO, YULI, JPIN, PING, MOTN, SHAN, TAPE, TAPO, TUNH, S105, ERPN, S104) were installed by IESAS, four continuous stations (JSUI, CHEN, LONT, TTUN) were operated by CWB, and one continuous station (TMAM) was organized by MOI. Most of the continuous stations have recorded data at least 2 years before the Chengkung earthquake, and the CSS were mostly surveyed annually (Table 1).

For the CSS data, we compared the campaigns 3 and 4 for determining the coseismic displacements (Table 1). The calibration of the postseismic displacements was applied to the campaigns 4 and 5 solutions. The first campaign of observed 60 stations was located mainly at northern part of the

Table 1. Summary of preseismic and postseismic GPS campaigns in the Longitudinal Valley area.

Campaign	Survey period	Number of stations*	Session (hrs)	Instrument
1	12–18 Mar. 2003 (DoY 070–076)	29/60	8	Trimble 4000 SSE/SSI
2	2–8 Jul. 2003 (DoY 183–189)	8/43	8	Trimble 4000 SSE/SSI
3	4–22 Nov. 2003 (DoY 308–326)	80/80	7	Trimble 4000 SSE/SSI
4	16–21 Dec. 2003 (DoY 350–355)	49/49	14	Trimble 4000 SSE/SSI
5	23 Mar–01 Apr. 2004 (DoY083–092)	65/115	14	Trimble 4000 SSE/SSI

*Number of station: number of stations used in this study/total occupancy number of stations.

Longitudinal Valley (LV), hence only 29 stations data near the epicenter area have been used for computing the coseismic displacement. The second campaign of measured 43 stations primarily surveyed a dense near-fault network at Juisui in the middle LV, hence only 8 stations data were utilized for estimating the coseismic displacement. Campaigns 3 and 4 occupied 80 and 49 stations respectively, distributed on the southern LV, hence all of the data were used in this study. Furthermore, campaign 5 measured all of the stations located on LV, except the stations surveyed by campaign 4.

For the data collection at each campaign, at least 8 stations were operated simultaneously. For instrument, we used dual-frequency geodetic GPS receivers (Trimble 4000 SSE/SSI Geodetic Surveyor). Each session contained 7 to 14 hours of observations with a 15-second sampling rate. The cutoff angle was 10 in elevation. Therefore, we systematically removed the obstruction to satisfy the satellite sky visibility. Before each field campaign, we also checked and adjusted the biases of the tribrach (leveling and centering) at the laboratory to reduce the centraling errors.

All of the data from CORS and CSS were processed into a daily solution through the standard procedures of the Bernese V4.2 software (Hugentobler *et al.*, 2001). We then combined daily solutions to a session solution, using the ADDNEQ program of the Bernese software. The normal equations were combined into a free network solution. The Paisha station (S01R) at Penghu in the Taiwan Strait was selected to define the "minimum constrained conditions" to its International Terrestrial Reference Frame 2000 (ITRF00) value. Our data processing procedures are listed below.

1) Apply the International GPS service (IGS) final orbit to reduce the effects of the orbit errors.

2) Introduce a correction of the antenna calibration table in the National Geodetic Survey (NGS), National Oceanic and Atmospheric Administration, U.S. Department of Commerce, and Astronomical Institute University of Bern, (AIUB) to reduce the effect of the phase center biases.

3) Adopt the double-differenced ionosphere-free linear combination of carrier phase observation to mitigate the first order ionospheric bias.

4) Compute the difference between the actual zenith delay based upon a standard atmosphere model (Saastamoinen, 1973) to determine the residual tropospheric zenith delay, then conducted estimates every 2 hours per station simultaneously with the station coordinates by least squares adjustment.

5) Constrain the daily solution to the Paisha station, at Penghu (S01R), which has a precise ITRF00 coordinate and is located in the stable Chinese continental margin.

6) Output the daily solution in Software Independent Exchange (SINEX) format.

4. Estimation of Coseismic Displacement

4.1 Regional coseismic displacements

Because the earthquake occurred at UTC 04 h 38 m, the estimation of the daily solution of the CORS on that day (DoY 344) did not include the data before the time of the earthquake. By comparing to the station position time series of the CORS from daily solutions before and after the Chengkung earthquake (DoY 344 and DoY 345), we obtained the coseismic displacement (Table 2). Significant displacements have been observed, in particular for the stations near the epicenter (e.g., station CHEN). By contrast, the northernmost station (JPEI) and the southernmost station (TMAM) were barely affected by the earthquake. In addition, we also calculated epoch by epoch displacements for determining coseismic displacement by applying kinematic positioning algorithms to obtain the instantaneous ground motion (Chen *et al.*, 2003). Figure 3 shows the epoch by epoch displacements at the CHEN, TUNH, TAPO and SHAN stations (with respect to station S01R) from 30-second sampling rate data. The differences of the coseismic displacements with that from the daily solution are also shown in Table 2.

A small difference (within a few millimeters) on the results between the epoch by epoch and daily solutions (Table 2) indicated that there were only very limited displacements after the main shock on that day. The difference at each station is generally within 6 mm of the displacement. Hence the coseismic displacement at CORS can be represented by either daily solution or kinematic positioning result. It is worthy noting that the coseismic displacements gradually increased towards the east, from the Longitudinal Valley to the epicenter area.

Compared to the CORS, the coseismic displacements of the CSS were more complicated to estimate. In this study, a two-step procedure has been used. For campaigns 1, 2 and 3, we applied preseismic station velocities (data from the years 2000 to 2003) to determine each expected station position on the day of the earthquake (DoY 344). For campaign 4, we utilized the nearby CORS station to calibrate the station position on the day of the earthquake for all other campaign-surveyed stations.

The data processing procedures for determination of the coseismic displacements with regard to the CSS are pre-

Table 2. Coseismic horizontal displacements from daily and epoch by epoch solutions due to the 2003 Chengkung earthquake in the CORS. The differences between two solutions are also shown.

Station	Daily solution		Epoch by epoch solution		Difference	
	N (mm)	E (mm)	N (mm)	E (mm)	N (mm)	E (mm)
CHEN	93.4±2.0	85.2±1.5	92.0±3.4	86.1±2.4	−1.4±3.9	0.9±2.8
ERPN	8.8±1.6	−36.8±1.2	12.4±2.3	−34.8±1.9	3.8±2.8	2.0±2.2
JPEI	6.2±1.9	−2.8±1.4	3.0±32.8	−5.8±2.7	−3.2±3.4	3.0±3.0
JPIN	29.0±1.8	7.0±1.4	30.6±2.4	9.6±2.1	1.6±3.0	2.6±2.5
KNKO	10.6±2.0	0.6±1.4	12.0±2.3	4.6±2.1	1.4±3.0	4.0±2.5
LONT	−10.0±1.8	−4.0±1.3	−8.5±2.3	−3.9±2.1	1.5±2.9	0.1±2.5
MOTN	−15.2±1.7	30.6±1.3	−14.3±1.7	29.8±1.8	0.9±2.7	0.8±2.2
PING	31.2±2.1	11.8±1.7	26.6±1.9	16.0±2.1	−4.6±3.3	4.2±2.7
S104	−32.2±1.6	−18.2±1.2	−29.5±1.8	−13.6±2.1	2.7±2.8	4.6±2.4
S105	−8.8±1.6	17.8±1.2	−5.4±1.6	16.5±2.0	2.6±2.8	−1.3±2.3
SHAN	2.4±1.7	24.0±1.3	5.6±2.5	23.4±2.0	3.2±3.0	−0.6±2.4
TAPE	25.6±1.7	−0.8±1.2	28.6±2.3	−1.5±2.1	3.0±2.9	−0.7±2.4
TAPO	43.2±1.7	−12.2±1.2	44.6±2.4	−7.8±2.1	1.4±2.9	4.4±2.4
TMAM	−8.4±1.7	4.0±1.2	−2.1±2.3	0.0±2.0	6.3±2.9	−4.0±2.3
TTUN	−15.8±1.8	2.6±1.4	−12.1±1.9	5.3±2.3	3.7±3.1	2.7±2.7
TUNH	93.2±1.8	41.8±1.3	91.0±2.6	41.4±2.2	−2.2±2.8	0.4±2.6
YULI	12.4±1.8	5.6±1.4	14.8±291	3.3±2.5	2.4±3.4	2.3±2.8

sented below.

1) Combine session solutions into campaign solutions.

2) Compute the preseismic station velocities for each CSS, using the data from 2000 to the end of 2003.

3) Subtract the preseismic station displacement between the observation day and the day of the earthquake (DoY 344) for the campaigns 1, 2 and 3.

4) Apply the postseismic displacements of the CORS between the dates of earthquake and the campaigns 4 to interpolate the CSS solution of campaign 4 on the day of the earthquake.

5) All coseismic station displacements relative to Paisha (S01R), Penghu are ultimately computed by constraining the S01R's ITRF00 coordinate system from those of the other stations.

From the results of the combined CORS and CSS stations, we found that the maximum horizontal coseismic displacement of about 126 mm occurred at station CHEN (around the epicenter) with 93.4 mm and 85.2 mm in the north and east components, respectively. The northernmost and southernmost stations at the CORS stations KNKO and TMAM had the least coseismic movement of 10.6 mm, 0.6 mm and −8.4 mm, 4.2 mm at the north and east components, respectively. The horizontal coseismic displacements with 95% confidence error ellipses for each of the GPS stations are plotted in Fig. 4. For the vertical coseismic movement, Fig. 10 shows the elevation changes in GPS height. All of the GPS stations were raised by the Chengkung earthquake. The largest uplifted GPS station was found at station S057 located to the south of the epicenter, with a 260 mm vertical uplift. The elevation changes, in general, decreased away from the epicenter area.

We can find a discontinuity on the vectors of the horizontal displacements along the eastern margin of the Longitudinal Valley which not surprisingly corresponds to the surface traces of the Chihshang fault and other segments of the LVF. To the east in the hanging-wall of the Coastal Range, from the north to the south, the station movements show a clear fan shape. The center of the fan of displacement vectors is between the stations S057 and S221, located at Tungho, about 7–8 km south of the epicenter. To the west on the footwall in the Central Range and the Longitudinal Valley, the movements indicate an opposite fan shape: the stations moved eastward near the latitude of the epicenter, and they moved northward or northwestward in the northern part and southward in the southern part of the Coastal Range, which is likely a mirror of the fan of the hanging-wall displacements.

4.2 Near-fault coseismic displacements

In order to understand the coseismic displacements in the near-fault area, we also included three dense-deployed GPS networks across the LVF from north to south, the Yuli network, Chihshang network and Luyeh network (Fig. 1).

Yuli network

Two CORS (YULI and JPIN) and 11 campaign-surveyed stations represent the dense Yuli network (Fig. 6). For three stations (0201, YULI and S039) in the Central Range, the coseismic displacements ranged from 14–17 mm with the NNE direction (24°–47°). For the stations in the Coastal Range (N681, JPIN, 0242, 0135 and S073), the displacements showed 30–52 mm in the directions of N to NNE (350°–21°). As a result, the relative displacement reaches 35 mm along the direction of NNE across the valley between the Central Range and Coastal Range.

Chihshang network

Four CORS (SHAN, TAPE, TAPO and TUNH) and 20

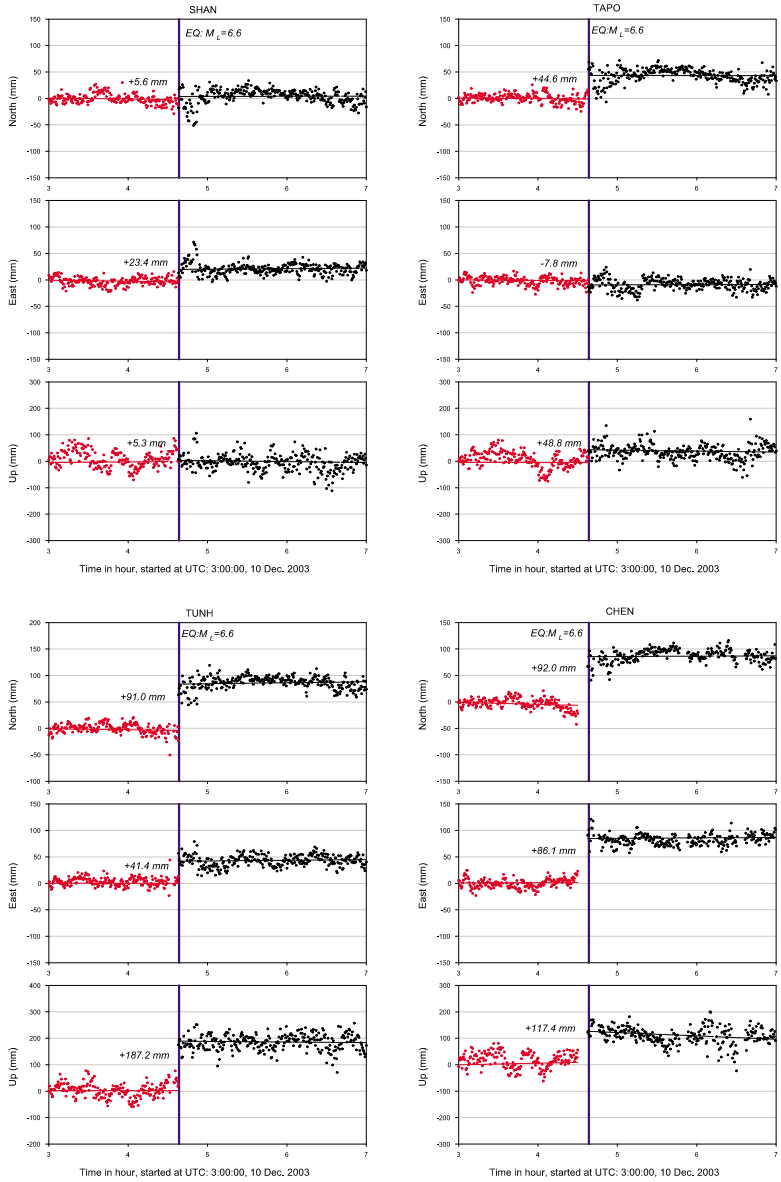

Fig. 3. The epoch by epoch displacements of the continuous GPS stations SHAN, TAPO, TUNH, and CHEN on 10 December 2003. For each subplot, the ordinate represents the north, east and up components of displacement from top to bottom, respectively, and the abscissa denotes the time at a 30 second sampling rate, beginning at UTC:03:00:00, 10 Dec. 2003 (units in hours).

campaign-surveyed stations constitute the Chihshang network (Fig. 7). In the northern part of the network, the stations (S224, S223 and S222) showed the displacements are 15–43 mm in the north direction (356°–5°). The relative displacement between the footwall and the hanging-wall was up to 28 mm. For the middle and southern part at the network, the displacements of the stations on the footwall side in the southern Central Range and Longitudinal Valley range from 24 mm to 45 mm in the direction of E to ESE (95°–123°). We can note that all stations in the footwall moved to the east. Larger displacements have been detected at stations on the hanging-wall in the Coastal Range, for example, 92.8 mm, 102.1 mm and 128.3 mm at stations N623, TUNH and S033, in N to NNE direction (9°–27°), respectively.

Because the Chihshang fault is responsible for the Chengkung earthquake, the Chihshang network provides a good opportunity to understand the near-fault coseismic deformation behavior. Three E-W profiles of stations were complied for comparisons (Fig. 7). The northern profile is composed of stations S168, TAPE and TAPO (Fig. 8(a)). The displacements are 33.6 mm, 25.6 mm and 44.9 mm at directions 112°, 358° and 344°, respectively. From west to east, the directions of the displacements changed dramatically counter-clockwise across the fault. The mechanism of the deformation across the fault was characterized by an oblique thrust movement with a significant left-lateral component. Similar behavior can be observed at the other two E-W profiles, SHAN, 0284, 0283 for the middle profile and S233, S230, S056 for the southern profile (Figs. 8(b) and (c)). The displacements are 24.1 mm, 19.1 mm, 68.6 mm and 29.9 mm, 20.0 mm, 58.6 mm with directions 84°, 21° and 341° and 126°, 68°, 317°, respectively.

Luyeh network

Table 3. Coseismic displacement of the 2003 Chengkung earthquake for CORS (in bold and italic) and CSS stations in southeastern Taiwan. D_N, D_E and D_U, north, east, and up components of the coseismic displacements, respectively; S, coseismic displacements; Azi_S, azimuth of S; a and b, semimajor and semiminor axes for the error ellipse of S; Azi_a, azimuth of a.

Station	Longitude (°)	Latitude (°)	D_N (mm)	D_E (mm)	S (mm)	Azi_S (°)	D_U (mm)	a (mm)	b (mm)	Azi_a (°)
0135	121.3404	23.2925	49.2	18.4	52.5	21	19.0±10.6	4.7	4.0	160
0201	121.3118	23.3558	12.6	9.2	15.6	36	0.4±11.7	5.3	4.3	157
0206	121.1011	22.8117	−18.6	−28.2	33.8	237	19.0±14.2	6.1	5.5	141
0207	121.1394	22.8196	−37.2	−45.4	58.7	231	66.0±9.6	4.2	3.7	143
0211	121.1339	22.7552	−24.8	−31.2	39.9	232	9.0±12.3	5.4	4.7	146
0235	121.2143	23.0985	14.4	15.0	20.8	46	36.8±14.7	6.9	5.1	146
0241	121.3267	23.3379	24.2	14.6	28.3	31	7.0±11.5	5.0	4.4	154
0242	121.3169	23.2978	42.0	10.6	43.3	14	7.6±12.1	5.1	4.8	152
0283	121.2254	23.1195	64.8	−22.6	68.6	341	117.0±12.8	5.6	4.9	145
0284	121.2180	23.1120	17.8	6.8	19.1	21	75.2±13.3	5.9	5.0	146
0308	121.1527	22.9439	−12.4	−5.6	13.6	204	34.0±15.6	6.5	6.3	134
1172	121.3075	23.2876	23.2	−2.0	23.3	355	21.2±15.3	6.9	5.6	157
1176	121.2934	23.2901	19.8	38.6	43.4	63	30.4±16.5	6.9	6.6	156
13R3	121.3167	23.3163	22.2	19.6	29.6	41	13.4±16.2	7.0	6.3	144
13R4	121.2907	23.3034	26.6	17.4	31.8	33	14.8±16.1	7.0	6.2	143
8049	121.1290	22.9476	−9.4	17.0	19.4	119	27.0±9.5	4.1	3.7	140
A038	121.4883	23.4528	19.4	−1.2	19.4	356	12.2±13.8	5.9	5.4	162
CHEN	121.3654	23.0992	93.4	85.2	126.4	42	154.4±4.5	2.1	1.6	162
ERPN	121.1580	22.9439	8.8	−36.8	37.9	283	71.4±3.7	1.8	1.3	154
HT63	121.1885	23.0976	−6.2	34.0	34.5	100	14.0±16.6	7.1	6.5	146
I138	121.1012	22.8665	−6.0	−31.2	31.8	259	11.0±9.9	4.2	3.9	146
JPEI	121.3632	23.5334	6.2	−2.8	6.8	336	5.0±4.0	1.9	1.4	173
JPIN	121.3507	23.3428	29.0	7.0	29.8	14	31.0±3.9	1.8	1.4	168
JSUI	121.4157	23.4937	15.4	−2.8	15.7	350	9.0±4.9	2.2	1.8	178
KNKO	121.4976	23.4740	10.6	0.6	10.6	3	23.8±4.1	2.0	1.4	173
LONT	121.1224	22.9081	−10.0	−4.0	10.8	202	51.4±4.2	2.0	1.5	152
MOTN	121.0187	23.2023	−15.2	30.6	34.2	116	11.6±3.9	1.8	1.4	159
N623	121.2839	23.0411	81.8	41.6	91.8	27	275.4±14.0	6.1	5.4	144
N681	121.3516	23.3847	29.6	−5.4	30.1	350	13.0±11.2	5.0	4.2	179
PING	121.4462	23.3212	31.2	11.8	33.4	21	39.6±4.9	2.2	1.8	166
S033	121.2717	23.1047	126.4	19.8	128.3	9	245.0±13.1	5.4	5.3	150
S039	121.2676	23.2781	11.2	12.2	16.6	47	11.2±13.4	6.0	5.0	173
S040	121.1418	23.0323	−3.2	34.0	34.2	95	27.0±12.2	5.3	4.7	144
S044	121.0143	22.6796	3.0	−5.8	6.5	297	15.0±10.7	4.7	4.1	143
S045	121.0724	22.8820	−12.4	0.0	12.4	180	16.0±13.8	6.1	5.2	143
S046	121.0467	23.1491	−24.6	36.8	44.3	124	14.2±12.2	5.3	4.7	149
S047	121.3513	23.4725	7.0	10.4	12.5	56	4.2±11.7	5.2	4.4	163
S054	121.1894	22.7958	−27.8	−34.0	43.9	231	2.0±9.9	4.3	3.8	146
S055	121.1147	23.1359	−21.6	39.6	45.1	119	48.0±14.3	6.3	5.4	140
S056	121.1904	23.0387	43.2	−39.6	58.6	317	76.0±13.5	6.0	5.1	148
S057	121.3011	22.9748	37.2	11.4	38.9	17	283.0±16.4	7.5	5.9	137
S059	121.5051	23.4902	19.4	4.4	19.9	12	12.2±11.5	5.0	4.4	19
S063	121.4704	22.6664	40.2	−39.6	56.4	315	13.0±12.9	6.0	4.6	146

Table 3. (continued).

Station	Longitude (°)	Latitude (°)	D_N (mm)	D_E (mm)	S (mm)	Azi_S (°)	D_U (mm)	a (mm)	b (mm)	Azi_a (°)
S072	121.1545	22.9273	−27.8	−85.0	89.4	252	46.0±10.6	4.6	4.1	144
S073	121.2799	23.2415	46.4	−5.6	46.7	353	59.0±12.3	5.3	4.8	166
S078	121.0370	23.1687	−9.2	42.4	43.4	102	32.0±15.6	6.5	6.3	141
S079	121.0187	23.2027	−21.6	19.8	29.3	137	15.0±12.3	5.6	4.5	145
S080	121.0050	23.2219	−15.6	17.0	23.1	132	13.0±12.8	5.6	4.9	145
S104	121.1813	22.8225	−32.2	−18.2	37.0	209	74.2±4.0	1.9	1.4	150
S105	121.1048	22.9534	−8.8	17.8	19.9	116	30.8±3.7	1.8	1.3	153
S121	121.4381	23.4990	15.8	9.6	18.5	31	32.6±12.0	5.3	4.5	0
S123	121.3820	23.5244	19.0	−4.2	19.5	348	59.6±12.0	5.2	4.6	178
S126	121.1423	22.8919	−6.2	−53.8	54.2	263	77.0±14.8	6.4	5.7	138
S149	121.3652	23.4316	14.2	−20.6	25.0	305	23.0±12.8	5.6	4.9	3
S168	121.1885	23.1326	−12.4	31.2	33.6	112	64.0±12.8	5.5	5.0	145
S194	121.1560	22.9447	6.2	−14.2	15.5	294	54.0±14.7	6.4	5.6	140
S197	121.1200	22.9392	−12.4	0.0	12.4	180	29.0±15.5	6.7	6.0	134
S198	121.1186	22.9405	−9.2	0.0	9.2	180	24.0±16.4	7.1	6.3	129
S200	121.1170	22.9055	−15.4	−8.4	17.5	209	28.0±16.6	7.4	6.2	129
S206	121.0838	22.9158	−6.2	5.6	8.4	138	8.0±15.1	6.6	5.8	138
S214	121.2324	22.9648	9.2	−25.6	27.2	290	257.0±14.7	6.4	5.6	144
S220	121.2964	22.9730	12.4	22.6	25.8	61	240.0±14.7	6.5	5.5	144
S221	121.2608	22.9301	−12.4	−19.8	23.4	238	205.0±14.2	6.3	5.3	140
S222	121.2413	23.1764	43.2	−2.8	43.3	356	92.0±14.0	6.1	5.4	147
S223	121.2368	23.1759	31.0	2.8	31.1	5	51.0±14.3	6.1	5.6	145
S224	121.2284	23.1796	15.4	0.0	15.4	0	47.0±15.1	6.7	5.7	142
S226	121.1974	23.1179	−6.2	28.4	29.1	102	41.0±14.4	6.2	5.6	144
S227	121.2106	23.0969	24.8	−14.0	28.5	331	90.0±15.4	6.7	5.9	142
S228	121.2017	23.1001	2.0	28.0	28.1	86	31.2±15.4	6.7	5.9	145
S229	121.1681	23.1032	−18.6	28.4	33.9	123	38.0±15.5	6.7	6.0	142
S230	121.1712	23.0359	7.4	18.6	20.0	68	11.0±15.4	6.7	5.9	141
S231	121.1648	23.0408	−14.2	35.6	38.3	112	9.0±15.4	6.6	6.0	142
S232	121.2089	22.9448	3.0	−31.0	31.1	276	236.0±14.5	6.4	5.5	143
S233	121.1518	23.0460	−17.6	24.2	29.9	126	13.0±14.7	6.3	5.7	143
S237	121.1413	22.8994	−12.4	−42.4	44.2	254	75.0±14.7	6.3	5.7	140
S239	121.0932	22.9071	−12.4	5.6	13.6	156	14.0±17.7	7.4	7.1	124
S240	121.0539	22.9008	−9.2	17.0	19.3	118	29.0±14.8	6.4	5.7	140
S241	121.0401	22.8942	−6.2	37.0	37.5	100	44.0±14.8	6.4	5.7	141
SANT	121.4082	23.1269	92.8	70.8	116.7	37	106.0±14.0	6.1	5.4	152
SHANN	121.1914	23.1106	2.4	24.0	24.1	84	36.4±3.9	1.8	1.4	159
TAPE	121.2227	23.1273	25.6	−0.8	25.6	358	69.2±3.7	1.8	1.3	160
TAPO	121.2293	23.1288	43.2	−12.2	44.9	344	73.6±3.7	1.8	1.3	160
TMAM	120.9994	22.6178	−8.4	4.2	9.4	153	2.2±3.7	1.8	1.3	160
TTUN	121.0726	22.7663	−15.8	2.6	16.0	171	19.2±4.6	2.1	1.7	148
TUNH	121.2921	23.0769	93.2	41.8	102.1	24	224.8±4.0	1.9	1.4	162
W048	121.1456	22.9031	0.0	−56.6	56.6	270	79.0±14.9	6.4	5.8	141
X307	121.1685	23.0895	−15.4	39.6	42.5	111	18.0±15.6	6.9	5.9	139
X308	121.2971	22.9784	6.0	31.0	31.6	79	237.4±16.0	7.0	6.1	142
YULI	121.2930	23.3427	12.4	5.6	13.6	24	31.2±4.0	1.9	1.4	165

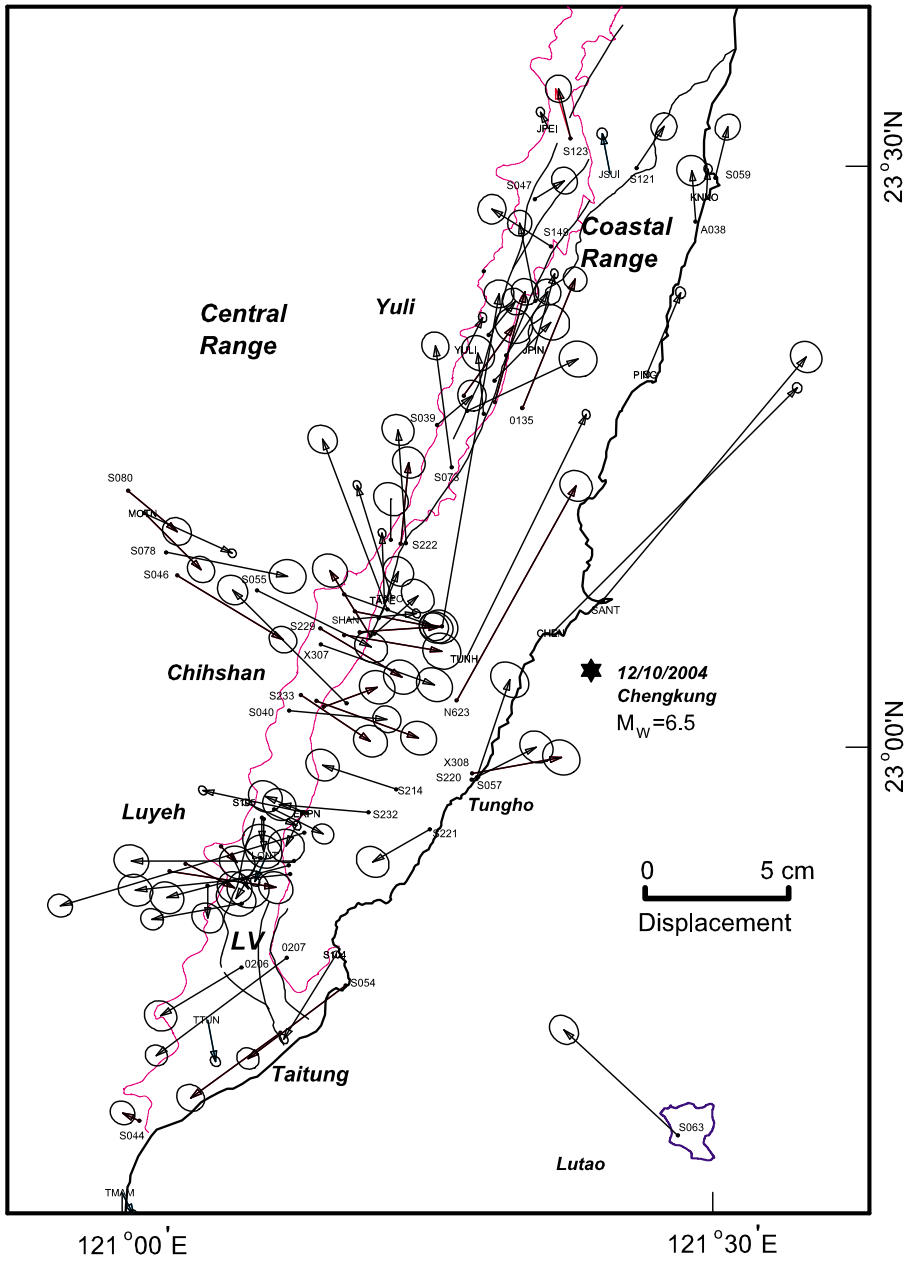

Fig. 4. Horizontal coseismic displacements relative to Paisha, Penghu. The 95% confidence error ellipse is shown at the tip of each coseismic vector. The epicenter is marked by a solid star. LV and LVF denote the Longitudinal Valley and Lnogitudinal Valley Fault, respectively.

Five continuous GPS stations (S105, LONT, ERPN, S104 and TTUN) and 21 campaign-surveyed stations make up the Luyeh network (Fig. 9). For the stations in the Central Range, the displacements range from 8 mm to 37 mm approximately in the ESE direction (100°–118°, Fig. 9). For the stations in the Longitudinal Valley, the displacements range 9-34 mm in the SW to S direction (180°–259°). The displacements of stations in the Coastal Range range from 23 mm to 89 mm in the SW to W direction (209°–283°).

The GPS data indicated two discontinuities for the coseismic horizontal displacements on both sides of the Longitudinal Valley in the Luyeh network. They correspond to two active faults: the Luyeh fault to the west and the Lichi fault to the east, which have been detected by previous geodetic measurements (Yu *et al.*, 1990; Lee *et al.*, 1998) and mapped by geomorphic analysis (Lee *et al.*, 1998; Shyu *et al.*, 2002).

5. Vertical Motions Across the Fault: Leveling and GPS Height

We have carried out two 10-km-long and one 3-km-long lines of repeated precise leveling across the southern Longitudinal Valley (Fig. 1). The two parallel 10-km-lomg lines of Luyeh network are located from Longtien to Luanshan, and from Yunglong to Juiyuan. The 3-km-long line is from Shihping to Fuli (Chihshang network). All of the benchmarks were surveyed with leveling and GPS observations. In addition, there are nearby continuous GPS stations which can be used to compare with the leveling results. The leveling surveys were conducted by a precise leveling procedure (Jackson *et al.*, 1983). Figure 10 shows the comparison of interseismic and postseismic leveling results with the GPS

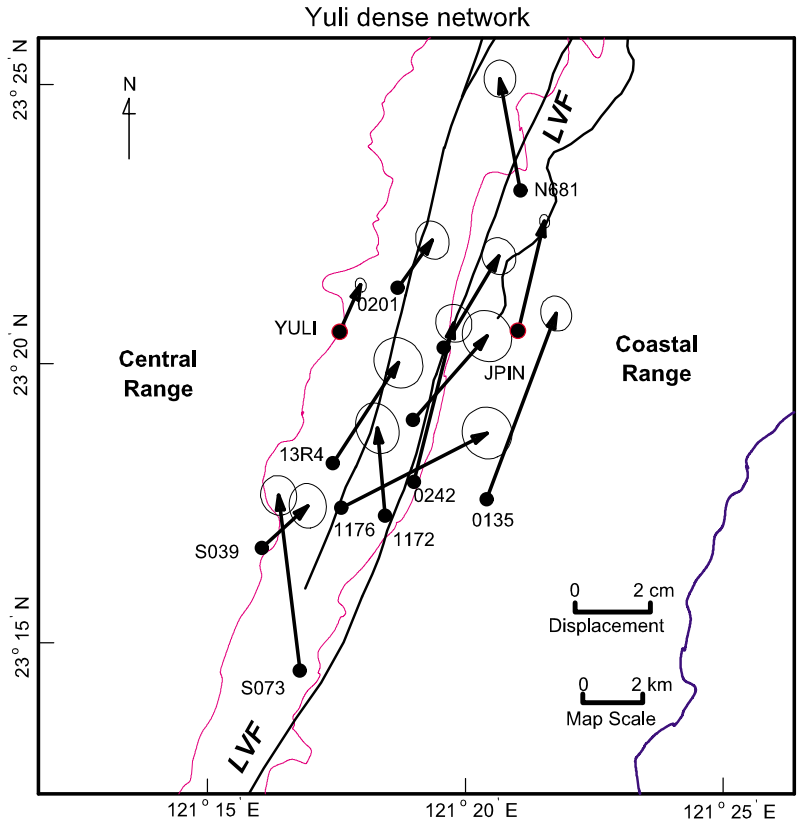

Fig. 5. Coseismic displacements relative to Paisha, Penghu for stations in the Yuli network. Notations are the same as in Fig. 4.

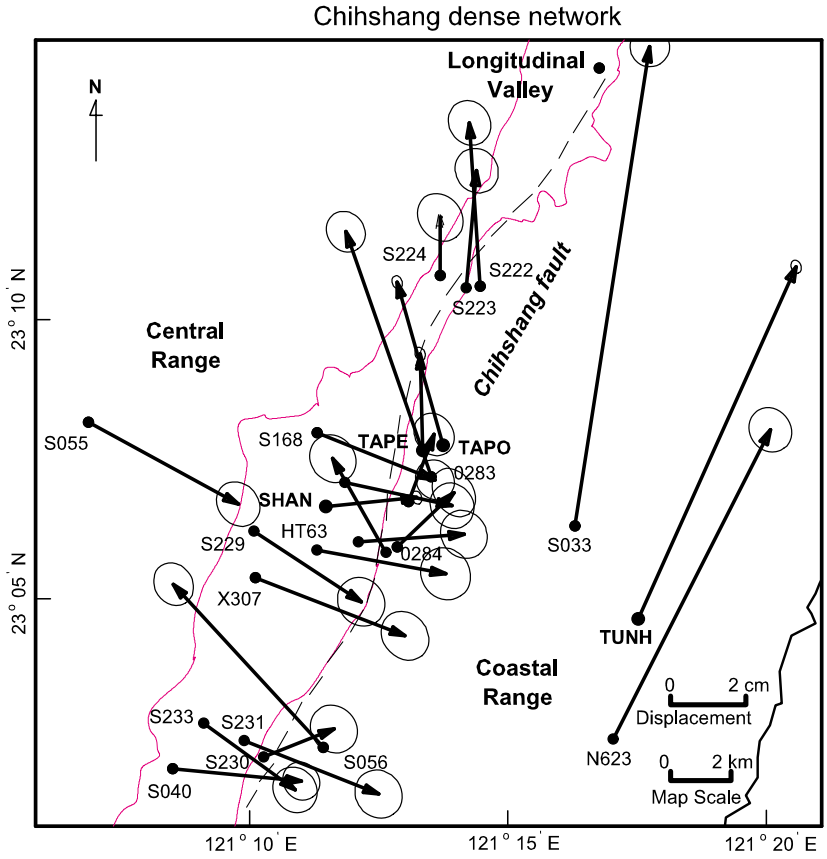

Fig. 6. Coseismic displacements relative to Paisha, Penghu for stations in the Chihahang network. Notations are the same as in Fig. 4.

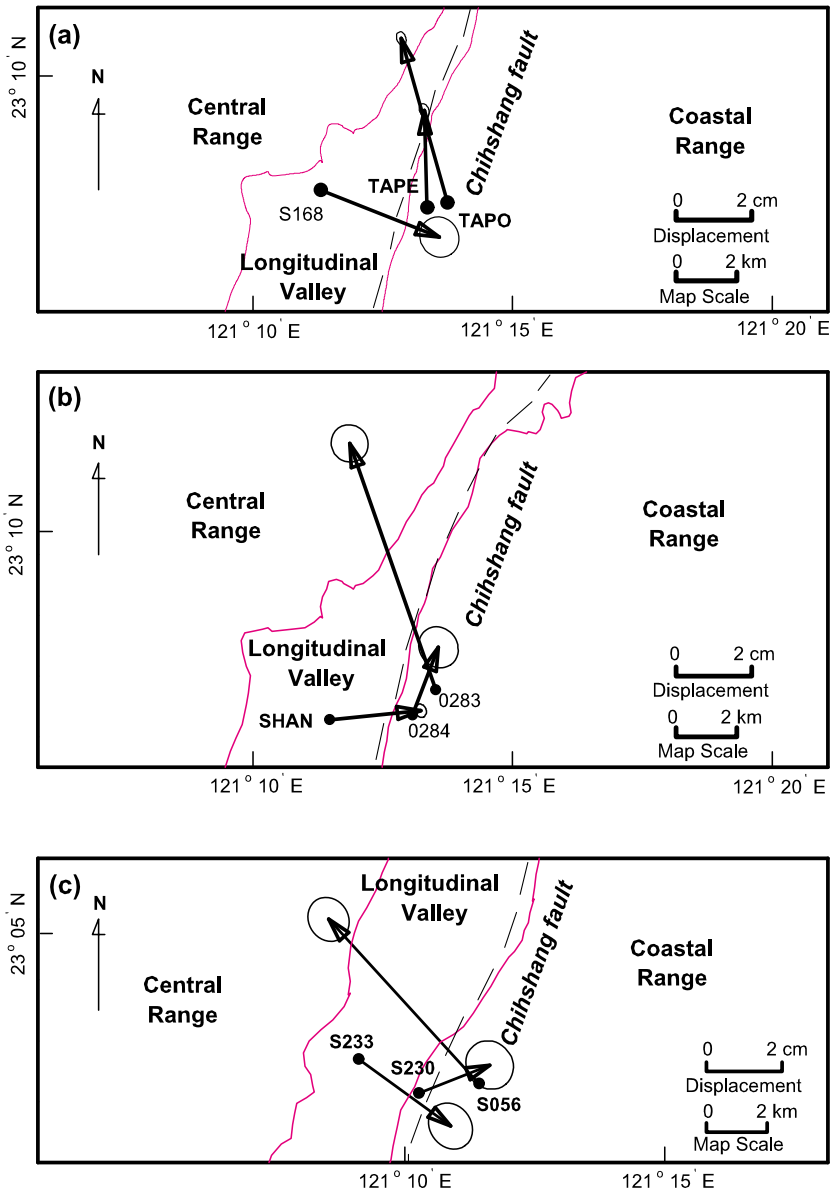

Fig. 7. Three profiles in the Chihshang network. Notations are the as in Fig. 6.

height on the two 10-km-long leveling routes in the Luyeh area.

The leveling and GPS height results reveal that the 2003 Chengkung earthquake produced a vertical offset of 80–110 mm (including co- and post-seismic deformation) for the Coastal Range relative to the Central Range in the Luyeh area. The Luyeh terrace across the Luyeh fault near Longtien was uplifted for about 30mm. A slight vertical offset of about 7 mm (S201–S203) was observed during the year 2002–2003 before the Chengkung earthquake across the Luyeh fault (Fig. 10).

The 3-km-long repeated precise leveling in the Chihshang area across the LVF was conducted after the Chengkung earthquake in February and March 2004 (Table 4). According to the leveling results from S224, S223 to S222, the accumulation of elevation change in one month reached 10 mm. Comparing with the GPS height of nearby CORS, TAPO, TAPE and SHAN in the same time period (Fig. 12(b)), the relative elevation change was 14 mm. Hence the elevation still changed drastically even three months after the earthquake.

6. Postseismic Displacement

6.1 Data analysis procedures

To better determine the postseismic displacements, we adopted two different strategies for the CORS and CSS in the data processing. For the CORS, estimating the daily solution and constraining S01R's ITRF00 coordinate system, the procedure was the same as the coseismic displacement algorithms. The results of the CORS provide detailed information for the temporal variations of postseismic deformation. The coordinates of the daily solution for each station were extracted from SINEX (Software INdependent EXchange) files to establish time series in the topocentric north-east-up (NEU) coordinate system. The NEU position data were synthesized and modeled independently in each of the three coordinate directions because correlations between components are very small (Zhang *et al*, 1997).

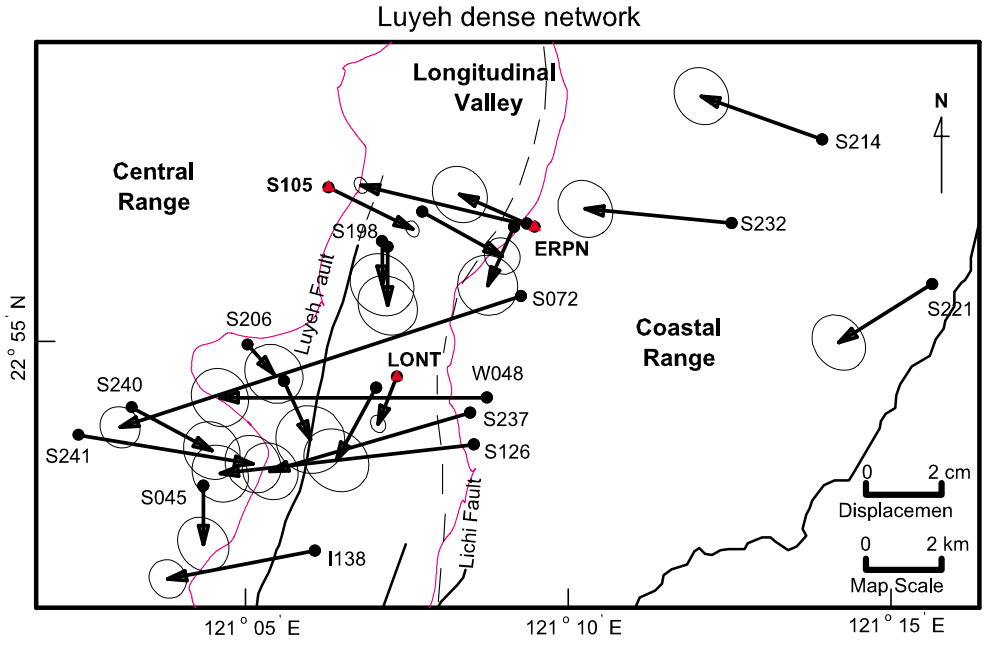

Fig. 8. Coseismic displacements relative to Paisha, Penghu for stations in the Luyeh network. Notations are the same as in Fig. 4.

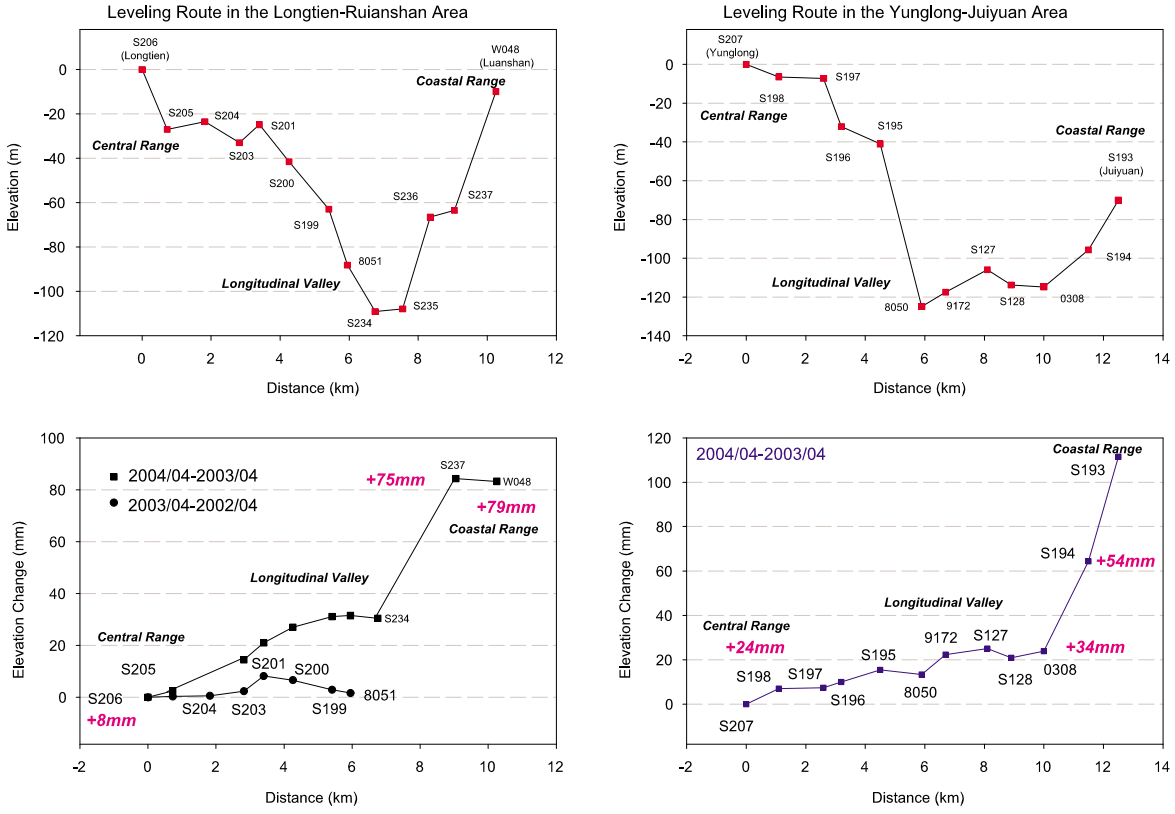

Fig. 9. The leveling results comparing with the GPS height of the interseismic and postseismic periods from April 2002 to April 2004. The abscissa represents the relative leveling route distance (units in km). The ordinate of the upper plots presents the elevation of the leveling route (units in m), and the y-axis of the lower plots expresses the elevation change of the leveling route (units in mm). The numbers in the subplot present the results of the GPS height, and there is less than 10 mm difference in the leveling results and GPS height.

The secular crustal deformation of the station during the 4 month period was removed by applying the 2000–2003 interseismic velocities.

For the CSS, the following interpolation method was used for campaign 4 (Table 1) whereby each of the station positions can be acquired on the day of the earthquake for all campaign stations. Combining session solutions into a campaign solution for campaign 5 can determine the total postseismic movement by using the campaign 5 solution subtracted from the interpolated data in

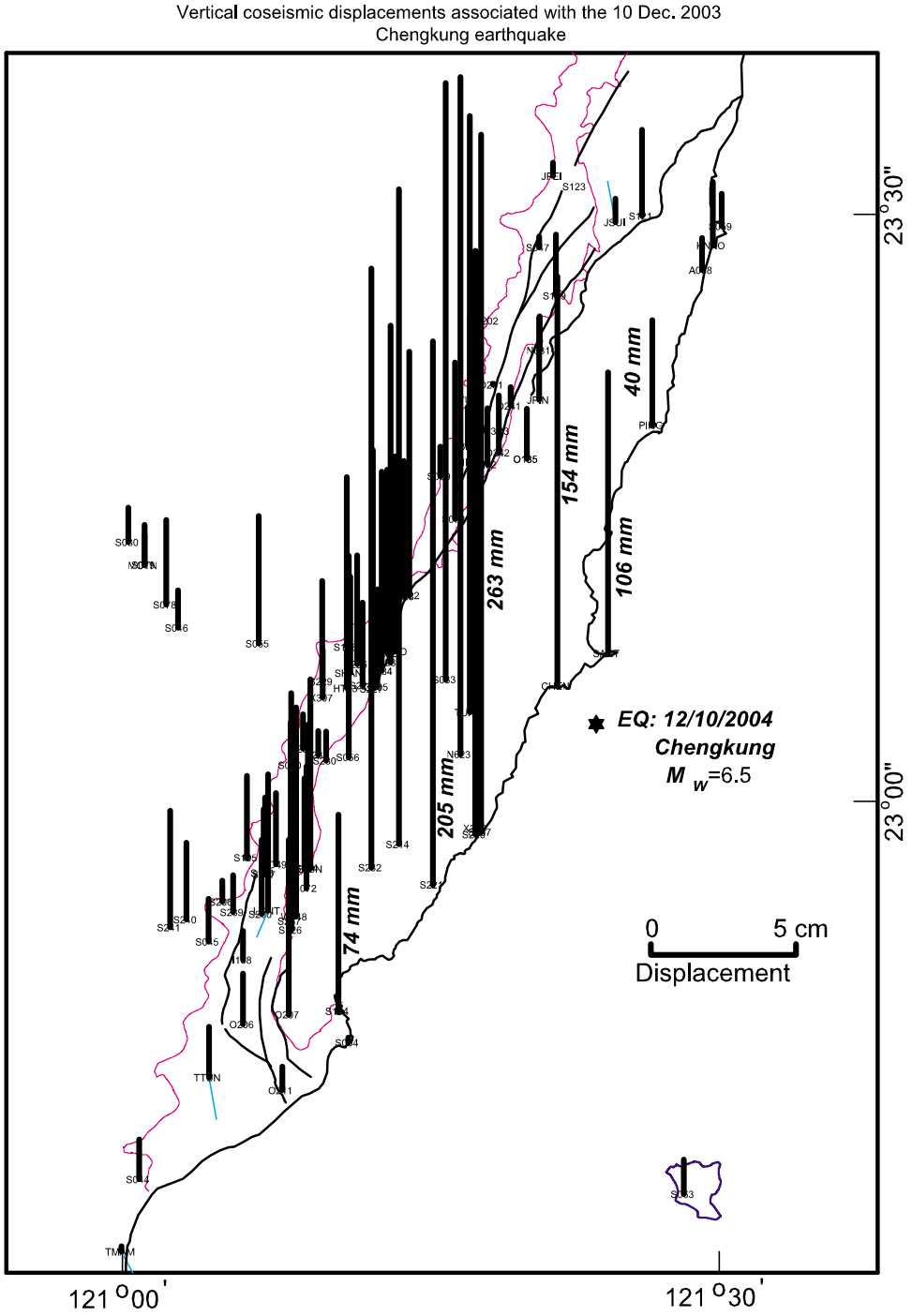

Fig. 10. The elevation changes in GPS height for the coseismic displacement.

campaign 4. To obtain the postseismic displacement, the secular crustal deformations of CSS were subtracted from each postseismic epoch prior to further analysis. The same process was used for the CORS. The procedures to determine the postseiesmic displacement is similar to that described previously for estimating coseismic displacement. The postseismic displacements about 4 months following the Chengkung earthquake are presented in Table 5.

6.2 Horizontal displacements

Larger postseismic horizontal displacements occurred near the surface trace of the LVF compared to the stations far from the fault. For example at the Chihshang network, the near-fault stations SHAN, TAPE, TAPO and 0283 moved 47–58 mm post-seismically. However, the stations on the footwall and on the hanging-wall of the LVF revealed different behavior in cosiemsic and postseismic displacements. The stations on the hanging-wall (TAPO and 0283) reached to 54 mm and 57 mm of the postseismic displacements in addition to the coseismic displacements of 45 and 68 mm. Alternately, the stations on the footwall (SHAN and TAPE) showed similar amounts of postseismic displacements up to 58 mm and 47 mm, but with relatively smaller coseismic displacements of 26 mm and 24 mm. It is obvious that the strain along the fault had not

Table 4. Leveling results at a short segment across the south LVF near Fuli.

Station	Dist. (km)	Observed elevation diff. Feb., 2004 (m)	Observed elevation diff. Mar., 2004 (m)	Elevation change (mm)
S222–S223	0.92	−25.12890	−25.13477	−5.87
S223–S224	1.50	+9.60627	+9.60136	−4.91

Table 5. Postseismic horizontal displacements about four months following the 2003 Cheng-Kung earthquake of the CORS (in bold and italic) and CSS in southeastern Taiwan. Disp., D_N and D_E, north and east components of the "raw" postseismic displacements, respectively; Vel., N, Vel., E, interseismic station velocities. Pos., D_N, D_E, north and east components of the "corrected" postseismic displacements, Pos., S, postseismic displacements; Azi_S, azimuth of Pos., S; a and b, semi-major and semi-minor axes for the error ellipse of S; Azi_a, azimuth of a.

Station	Disp., D_N (mm)	Disp., D_E (mm)	Vel., N (mm/yr)	Vel., E (mm/yr)	Pos., D_N (mm)	Pos., D_E (mm)	Pos., S (mm)	Azi_S (°)	a (mm)	b (mm)	Azi_a (°)
0135	26.1	8.9	49.7	−54.1	11.8	24.5	27.2	64	2.2	2.0	7
0201	7.7	−6.1	29.6	−45.4	−0.8	7.0	7.0	97	2.2	1.9	154
0283	70.0	−26.9	49.0	−53.3	55.9	−11.6	57.1	348	1.7	1.5	176
0284	18.6	−8.6	46.4	−47.1	5.3	4.9	7.2	43	1.9	1.7	171
13R3	9.2	0.0	35.6	−63.3	−1.0	18.2	18.2	93	2.3	2.1	171
CHEN	35.5	6.7	48.3	−55.7	21.6	22.7	31.4	46	0.7	0.5	163
ERPN	23.4	−34.6	58.3	−55.0	6.6	−18.8	19.9	289	0.6	0.4	155
I138	−9.2	11.4	25.0	−45.4	−16.4	24.5	29.4	124	2.1	2.0	152
JPEI	9.7	6.9	33.3	−38.3	0.1	17.9	17.9	89	0.6	0.5	173
JPIN	23.1	−2.7	49.4	−47.3	8.9	10.9	14.1	50	0.6	0.5	168
KNKO	22.8	−9.6	51.9	−54.8	7.9	6.2	10.0	38	0.6	0.5	173
LONT	−2.5	−1.5	22.0	−30.0	−8.8	7.1	11.3	141	0.7	0.5	155
MOTN	−10.4	4.6	14.0	−38.0	−14.4	15.5	21.2	133	0.6	0.4	160
N681	16.9	−3.7	48.0	−45.0	3.1	9.2	9.7	72	2.2	2.0	177
PING	28.5	−3.2	53.0	−53.8	13.3	12.3	18.1	43	0.7	0.6	167
S033	51.5	25.0	49.0	−49.3	37.4	39.2	54.2	46	2.0	1.9	155
S039	6.2	14.2	35.2	−39.3	−3.9	25.5	25.8	99	2.5	2.2	3
S055	−4.2	7.4	23.5	−37.9	−11.0	18.3	21.3	121	2.0	1.8	154
S056	15.6	−19.8	46.7	−54.4	2.2	−4.2	4.7	298	1.9	1.8	149
S072	17.4	−48.8	44.0	−53.2	4.7	−33.5	33.8	278	2.1	1.9	148
S073	18.6	2.8	41.7	−48.2	6.6	16.7	17.9	68	2.2	2.1	164
S104	6.7	−25.8	45.1	−50.3	−6.3	−11.3	13.0	61	0.6	0.4	151
S105	−10.2	14.7	22.1	−31.5	−16.6	23.8	29.0	125	0.7	0.5	155
S200	3.0	−2.8	36.0	−40.2	−7.4	8.8	11.4	130	2.8	2.5	123
S220	31.8	3.0	52.7	−67.1	16.6	22.3	27.8	53	2.3	2.0	157
S239	−3.0	−2.8	22.0	−30.0	−9.3	5.8	11.0	148	2.6	2.4	124
SHAN	−14.6	43.1	26.3	−37.5	−22.2	53.9	58.3	112	0.6	0.5	160
TAPE	−22.5	25.5	28.3	−36.9	−30.6	36.1	47.4	130	0.6	0.4	161
TAPO	66.8	−9.7	45.1	−50.1	53.8	4.7	54.0	5	0.6	0.4	161
TMAM	00.0	−6.3	12.4	−29.8	−3.6	2.3	4.2	147	0.7	0.6	151
TTUN	−1.9	−6.1	10.2	−34.9	−4.8	3.9	6.2	141	0.6	0.5	150
TUNH	45.3	19.2	41.2	−44.5	33.4	32.0	46.3	43	0.6	0.5	163
YULI	7.5	−6.1	30.6	−37.7	−1.3	4.7	4.9	105	0.7	0.5	166

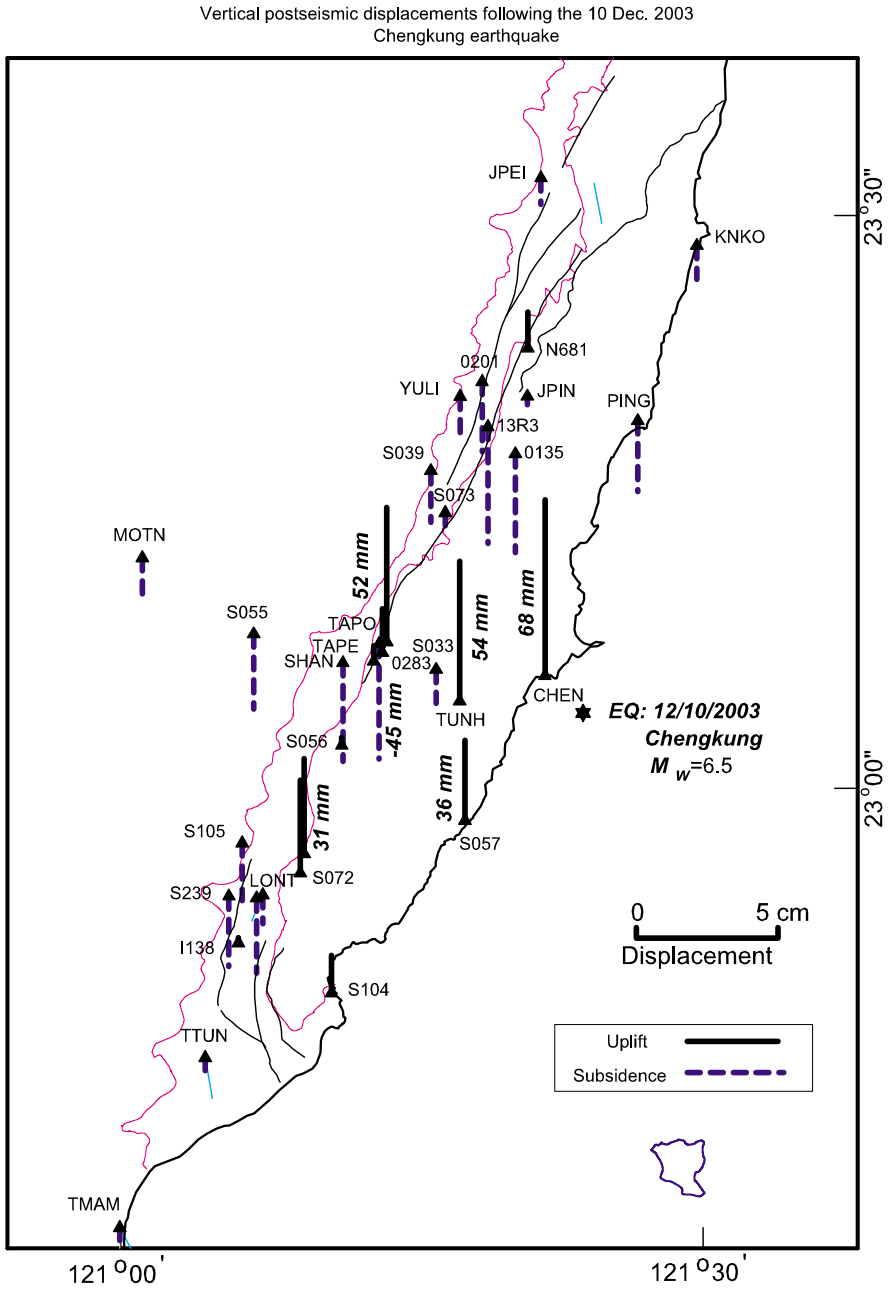

Fig. 11. The elevation changes in GPS height for the posteismic displacements, the solid bars denote uplift and the dash bars represent subsidence.

been totally released by the main shock of the earthquake near the surface. Hence the postseismic deformation exhibited a rapid movement around the surface of LVF during at least a four-month period. From the hanging-wall side to the footwall side at the latitude of the epicenter, the stations CHEN, TUNH, S033, TAPO, and 0283 showed an increasing trend of the postseismic displacements of 31 mm, 46 mm, 54 mm, 54 mm and 57 mm, respectively.

6.3 Vertical movements

With regard to the elevation change of the postseismic movements in the regional sense, the stations near the epicenter moved upward (the solid bars in Fig. 11), and other stations moved downward (the dash bars in Fig. 11). The maximum uplift of the postseismic movements occurred at station CHEN with a 68 mm elevation change. The maximum subsidence of the postseismic movements was at station 13R3 with 45 mm change. The largest relative elevation change of the poseismic movement occurred across the LVF between the stations TAPE and TAPO with about a 100 mm change in 109 days after the main shock.

6.4 Near fault post-seismic deformation

To better understand the near fault postseismic displacements, three continuous station pairs have been plotted in Fig. 12. From the north to the south, they are YULI-JPIN (Yuli network), SHAN-TAPO (Chihshang network) and S105-ERPN (Luyeh network). The distances between the two stations for each pair are 5.9 km, 3.7 km, 4.3 km and 5.6 km, respectively.

The relative coseismic displacement of the Yuli network (Fig. 12(a)) can be denoted by N-E-U components: +16.6 mm, +1.1 mm, and −0.5 mm for the north, east and up components, respectively. The three components for the

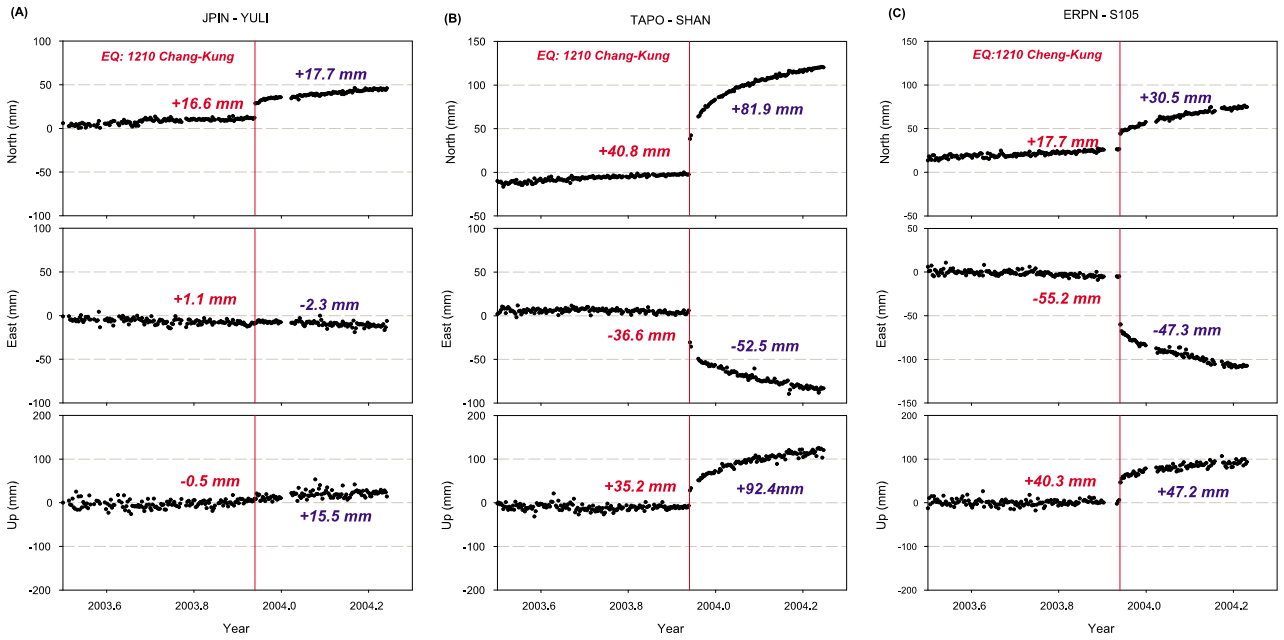

Fig. 12. Position variations in four near fault station pairs, ordered in YULI-JPIN, SHAN-TAPO and S105-ERPN. For each subplot, the abscissa denotes the time in year, and the ordinate are the north, east and up components of each baseline, respectively. The central vertical line in each subplot indicates the time of the earthquake, the number in the left hand side of the line expresses the relative coseismic displacement and the number in the right hand side of the line means the relative postseismic displacement of the earthquake.

relative postseismic displacement are +17.7 mm, −2.3 mm and 15.5 mm, respectively.

For the Chihshang network (Fig. 12(b)), the relative coseismic displacements are +40.8 mm, −36.6 mm and +35.2 mm for the north, east and up components, respectively. For the relative postseismic displacement, they are +81.9 mm, −52.5 mm and +92.4 mm, respectively.

For the southernmost Luyeh network (Fig. 12(c)), the N-E-U components of the relative coseismic displacements are +17.7 mm, −55.2 mm and +40.3 mm for the north, east and up components, respectively. For the relative postseismic displacement of the earthquake, they are +30.5 mm, −47.3 mm and +47.2 mm, respectively.

In summary, it appears that the surface postseismic displacement of the earthquake near the LVF had the largest amount in the Chihshang network, which is more than two times that of the coseismic displacement. The station pair in the Luyeh network, which is located 20 km south of Chihshang, also had a significant postseismic displacement. However, the northernmost station pair YULI-JPIN of the Yuli network, which is located 20 km north of Chihshang, showed a relatively small amount of postsiesmic slip. We interpret that the Yuli segment, an active fault segment north of the Chihshang fault, had less effect of rupturing caused by the Chengkung earthquake.

7. Conclusions

We have obtained coseismic and postseismic deformation of the 2003 M_w 6.5 Chengkung earthquake resulting from rupturing of the Chihshang fault, a segment of the LVF, based on analyses of more than 2 years of GPS data (CORS and CSS) and three leveling routes.

From aspect of GPS data processing, by analyzing the results of daily solution and kinematic positioning, only slight differences have been found between epoch by epoch coseismic displacements and daily solution results to within a few millimeters.

For the coseismic horizontal displacements in the hanging-wall of the Chihshang fault, the movements revealed a distinct fan shape with vectors toward N-NNE in the northeast, NW-W in the middle-west, NE-NEE in the middle-east and SW in the south. The maximum coseismic horizontal displacement of about 126 mm occurred around the epicenter. The center of the fanwas located about 5–8 km south of the epicenter near Tungho.

In the footwall, the coseismic movements showed an opposite fan-shape distribution with vectors towards N-NNE in the north, E-ESE in the middle, and SE-SSE in the south. The maximum coseismic horizontal displacement of the footwall occurred about 45 mm in the middle, a few kilometers west of the LVF.

For the vertical movement, all stations were uplifted by the coseismic effects in the study area with the largest vertical uplift of 260 mm near the epicenter. During the subsequent postseismic movements, the stations near the epicenter continued to move upward. However, other stations elsewhere moved downward. The largest relative postseismic elevation change occurred across the surface trace of the Chihshang fault, with about 100 mm of vertical offset.

From the epicenter toward the LVF (from the hanging-wall toward the footwall), the stations showed an increasing trend of postseismic movements. A larger postseismic movement closer to the LVF implies that the slip of the coseismic rupturing was not totally released the strain through the surface level of the LVF. From three pairs of GPS continuous stations across the LVF, the middle pair SHAN-TAPO (the Chihshang network), and the southern pair S105-ERPN (the Luyeh network), have a more signif-

icant postseismic movement than the northern pair YULI-JPIN (the Yuli network), which is located across the Yuli fault, another active segment of the LVF.

Acknowledgments. The authors would like to express their sincere gratitude to their colleagues of Geodetic Group at IESAS and the assistants for their contribution to the GPS field work and procurement of continuous GPS data from the permanent stations. The generous provision of continuous GPS data by the MOI and CWB as well as precise ephemeredes of GPS satellites by the IGS community is greatly appreciated. We also thank J. C. Lee, R. J. Rau and an anonymous reviewer for their valuable comments. This work benefited from the grants of National Science Council (NSC92-2119-M-001-016) and is a contribution of Institute of Earth Sciences, Academia Sinica, IESASXXX.

References

Angelier, J., H. T. Chu, and J. C. Lee, Shear concentration in a collision zone: kinematics of the active Chihshang Fault, Longitudinal Valley, eastern Taiwan, *Tectonophysics*, **274**, 117–144, 1997.

Angelier, J., H. T. Chu, J. C. Lee, and J. C. Hu, Active faulting and earthquake risk: the Chihshang Fault case, Taiwan, *J. Geodynamics*, **29**, 151–185, 2000.

Barrier, E., J. Angelier, H. T. Chu, and L. S. Teng, Tectonic analysis of compressional in an active collision zone: the deformation of Pinanshan Conglomerates, eartern Taiwan, *Proc. Geol. Soc. China*, **25**, 123–138, 1982.

Bock, Y., R. M. Nikolaidis, P. J. de Jonge, and M. Bevis, Instantaneous geodetic positioning at medium distances with the Global Positioning System, *J. Geophys. Res.*, **105**, 28,223–28,253, 2000.

Broadband array in Taiwan for seismology (BATS), http://bats.earth.sinica.edu.tw/, 2003.

Central Weather Bureau (CWB) earthquake report, http://www.cwb.gov.tw/V4e/index.htm, 2003.

Chen, H. Y., L. C. Kuo, W. S. Chung, and S. B. Yu, Using Quasi Ionosphere-Free Post-Processing Algorithm on The Medium-Range Kinematic High Accuracy GPS Relative Positioning, *Wuhan University Journal of Natural Sciences*, **8**(2b), 610–618, 2003.

Cheng, L. W., J. C. Lee, Y. M. Wu, and J. C. Hu, Inversion of coseismic deformation of Chengkung Earthquake in eastern Taiwan revealed by strong motion and continuous GPS, in *AGU Fall Meeting*, San Francisco, 2004.

Hugentobler, U., S. Schaer, and P. Fridez, Bernese GPS software Version 4.2, 515 pp., Astro. Inst., Univ. of Berne, Berne, Switzerland, 2001.

Hwang, C. W., L. H. Lee, S. B. Yu, and H. Y. Chen, Single and multi-epoch analyses of GPS baseline network: Application to coordinate and velocity determinations in central Taiwan, *J. Surv. Eng.*, **130**(2), 86–94, 2004.

Jackson, D. D., A. Cheng, and C. C. Liu, Tectonic Motions and systematic Errors in Leveling and Trilateration Data for California, *Tectonophysics*, **97**, 73–83, 1983.

Lee, J. C. and J. Angelier, Localisation des d'eformations actives et traitements des données géodésiques: l'example de la faille de la Vallée Longitudinal, Taïwan, *Bull. Soc. Géol. France*, **164**(4), 533–540, 1993.

Lee, J. C., J. Angelier, H. T. Chu, S. B. Yu, and J. C. Hu, Plate-boundary strain partitioning along the sinistral collision suture of the Philippine and Eurasian plates: Analysis of geodetic data and geological observation in southeastern Taiwan, *Tectonics*, **17**(6), 859–871, 1998.

Lee, J. C., J. Angelier, H. T. Chu, J. C. Hu, F. S. Jeng, and R. J. Rau, Active Fault Creep Variations at Chihshang, Taiwan, Revealed by Creepmeter Monitoring, 1998–2001, *J. Geophys. Res.*, **108**(B11), 2528, doi:10.10129/2003JB002394, 2003.

Page, B. M. and J. Suppe, The Pliocene Lichi melange of Taiwan: its plate-tectonic and olistostromal origin, *Amer. Jour. Sci.*, **281**, 193–227, 1981.

Remondi, B. W. and G. R. Brown, Triple differencing with Kalman filtering: Make it work, *GPS Solution*, **3**(3), 58–64, 2000.

Saastamoinen, I. I., Contribution to the theory of atmospheric refraction, *Bull. Geod.*, **107**, 13–24, 1973.

Shyu, J. B. H., K. Sieh, L. H. Chung, Y. G. Chen, and Y. Wang, The active tectonics of eastern Taiwan-new insights from the two geomorphic tablelands ("the Feet") in the Longitudinal Valley, *EOS, Trans., Am. Geophys. Uni.*, **83**(47), Fall Meet. Suppl., Abstract T61B–1278, 2002.

Smith, S. W. and M. Wyss, Displacement on the San Andreas fault subsequent to the 1966 parkfield earthquake, *Bull. Seism. Soc. Am.*, **58**, 1955–1973, 1968.

Teng, L. S. and Y. Wang, Island arc system of the Coastal Range, eastern Taiwan, *Proc. Geol. Soc. China*, **24**, 99–112, 1981.

Williams, P. L. and H. W. Magistrale, slip along the Superstition Hills fault associated with the 24 November 1987 Superstition Hills, California, earthquake, *Bull. Seismol. Soc. Am.*, **79**, 390–410, 1989.

Yu, S. B. and L. C. Kuo, Present-day crustal motion along the Longitudinal Valley fault, eastern Taiwan, *Tectonophysics*, **333**, 199–217, 2001.

Yu, S. B. and C. C. Liu, Fault creep on the central segment of the Longitudinal Valley fault, eastern Taiwan, *Proc. Geol. Soc. China*, **32**(3), 209–231, 1989.

Yu, S. B., D. D. Jackson, G. K. Yu, and C. C. Liu, Dislocation model for crustal deformation in the Longitudinal Valley area, eastern Taiwan, *Tectonophysics*, **183**, 97–109, 1990.

Yu, S. B., G. K. Yu, L. C. Kuo, and C. Lee, Crustal deformation in the southern Longitudinal Valley area, eastern Taiwan, *J. Geol. Soc. China*, **35**(3), 219–230, 1992.

Yu, S. B., H. Y. Chen, and L. C. Kuo, Velocity field of GPS stations in the Taiwan area, *Tectonophysics*, **274**, 41–59, 1997.

Yu, S. B., Y. J. Hsu, L. C. Kuo, H. Y. Chen, and C. C. Liu, GPS measurement of postseismic deformation following the 1999 Chi-Chi, Taiwan, earthquake, *J. Geophys. Res.*, **108**(B11), 2520, 10.1029/2003JB002396, 2003.

Zhang, J., Y. Bock, H. Johnson, P. Fang, S. Williams, J. Genrich, S. Wdowinski, and J. Behr, Southern California Permanent GPS Geodetic Array: Error Analysis of Daily Position Estimates and Site Velocities, *J. Geophys. Res.*, **102**(B8), 18035-18055, 1997.

H.-Y. Chen (e-mail: chenhy@earth.sinica.edu.tw), S.-B. Yu, L.-C. Kuo, and C.-C. Liu